PNAS
www.pnas.org

Supplementary Information for

The Seawater Carbon Inventory at the Paleocene-Eocene Thermal Maximum

Laura L. Haynes*[1,2,3] and Bärbel Hönisch[1,2]

[1] Department of Earth and Environmental Sciences, Columbia University, New York, NY

[2] Lamont-Doherty Earth Observatory of Columbia University, Palisades, NY

[3] Now at Department of Earth Science and Geography, Vassar College, Poughkeepsie, NY

*Corresponding Author email: lhaynes@vassar.edu

This PDF file includes:

Supplementary text
Figures S1 to S9
Legends for Datasets S1 to S5
SI References

Other supplementary materials for this manuscript include the following:

Datasets S1 to S5

www.pnas.org/cgi/doi/10.1073/pnas.2003197117

Supplementary Information Text

1. Sensitivity of reconstructed DIC to input parameters

In order to assess the uncertainties that our input assumptions imply for our DIC reconstruction, we conducted a series of sensitivity studies, where: 1) ΔT ranges from 3-6°C[1], 2) S stays constant across the excursion, 3) seawater $[B]_T$ is higher (at the modern value, 432 μmol/kg), 4) background pH is lower (7.67[2] instead of 7.8[3]), and 5) background seawater DIC is higher, according to the pre-PETM baseline of the LOSCAR model runs of ref. 3 (1920 μmol/kg, Fig. S2). S, T, and $[B]_T$ impose a negligible impact on our resultant reconstructed DIC values. Background DIC and pH also impose a somewhat larger effect, with both causing an overall increase in the magnitude of the DIC excursion. We further note that the culture calibrations used here were conducted at a seawater Mg/Ca (Mg/Ca_{sw}) =1.5 mol/mol, which has been estimated for the Paleocene ocean[4,5]. Because this value is not precisely known, this introduces an additional factor of uncertainty in our estimates. However, because 1.5 mol/mol is a lower end member estimate for Mg/Ca_{sw}[e.g. 4,6], our calibration offers a maximum estimate of B/Ca sensitivity to $[B(OH)_4^-/DIC]$ and minimum estimates of DIC change. Uncertainty in input parameters therefore does not change our fundamental conclusion that DIC increased by at least +360 μmol/kg from a prescribed pre-PETM DIC of 1760 μmol/kg to at least 2,120 μmol/kg during the peak-PETM (Dataset S1).

2. Sensitivity of $\delta^{13}C_{source}$ to input parameters

The input assumptions of this analysis do not significantly influence our mean calculated $\delta^{13}C_{source}$. We make a reasonable estimate of pre-PETM oceanic $\delta^{13}C$ based on records of the benthic foraminifer *Nutallides truempyi*[7], whose shell $\delta^{13}C$ will not be affected by symbiont activity and surface ocean productivity, unlike many planktic foraminifer species. We use mean value of 1‰, which also agrees with the pre-PETM estimates of oceanic $\delta^{13}C$ by ref. 3. Choice of pre-PETM $\delta^{13}C$ makes a negligible difference on calculated $\delta^{13}C_{source}$ (Fig. S4). While a wide variability is observed in surface ocean $\delta^{13}C$ records of

the CIE (-0.7‰ to –4.4‰, compiled by ref. 10) and it has been proposed that the true surface ocean CIE has been affected by diagenetic overprinting (yielding a CIE of -4.6‰[8]), we here use our reconstruction to infer the total oceanic DIC reservoir change and therefore adopt the whole-ocean estimate of -3.5‰[9]. Furthermore, recent work using Archaeal lipid biomarker $\delta^{13}C$ has pinpointed the global CIE magnitude at 4.0 $\pm$ 0.4‰[10]. However, if we do assume a larger CIE magnitude of -4.6‰, our reconstruction yields a mean $\delta^{13}C_{source}$ estimate of -13.0‰, still invoking predominant contributions from volcanic carbon. Finally, our assumed surface-deep ocean DIC gradient (260 µmol/kg from surface to deep[11]) and therefore overall ocean DIC reservoir size has the potential to influence $\delta^{13}C_{source}$ via the mass balance equation (2). If the DIC gradient changed across the PETM, sedimentary evidence suggests that it would have steepened, as barite accumulation records from Site 1209 and other locations indicate an increase in export production during the peak-PETM[12]. Because we extrapolate from surface ocean DIC, this would cause us to under-estimate peak-PETM whole ocean DIC and again require an even less negative $\delta^{13}C_{source}$. Finally, assuming a pre-event surface ocean DIC value of 1920 µmol/kg as prescribed in the LOSCAR model[2] would yield a larger DIC inventory, but our calculated DIC excursion would also be slightly greater (mean= +1260 µmol/kg), corresponding to the same mean predicted $\delta^{13}C_{source}$ (-10‰).

3. Model-Data comparison across the PETM recovery

In addition to the large magnitude of the DIC increase at the PETM onset, the structure of the recovery interval can also yield interesting insight into carbon burial processes and PETM mitigation. The structure of this DIC excursion depends on both $\delta^{11}B$-derived pH and measured B/Ca. In comparing both proxy records, we note that B/Ca recovers more rapidly than $\delta^{11}B$ and sustained low pH-values are responsible for decreasing DIC at 40 kyr post-CIE (Fig. 1A-B, D). In contrast, the ultimate pH recovery at relatively constant B/Ca drives the secondary DIC increase at 150 kyr post-CIE, as higher DIC is required to explain the relatively lower B/Ca values compared to $\delta^{11}B$.

In addition, proxy-derived DIC estimates recover faster than modeled DIC excursions (Fig. 3A). At face value, this suggests more rapid oceanic carbon removal during the recovery phase than models predict. However, the fast recovery that we reconstruct here may instead yield from the fact that B/Ca data during the recovery phase from Site 1209 show a wide range of variability (Fig. 1B). In comparison, surface-dwelling *Acarinina spp.* from the same site record lower B/Ca values during the recovery, while the peak-PETM excursion is similar in magnitude (71-45 and 70-45 μmol/mol in *Acarinina* and *Morozovella*, respectively)[13]. Therefore, further paired high-resolution B/Ca and $\delta^{11}B$ records will be necessary to constrain the recovery of ocean DIC as weathering and organic carbon burial feedbacks mitigated the PETM C excursion.

Supplementary Figures

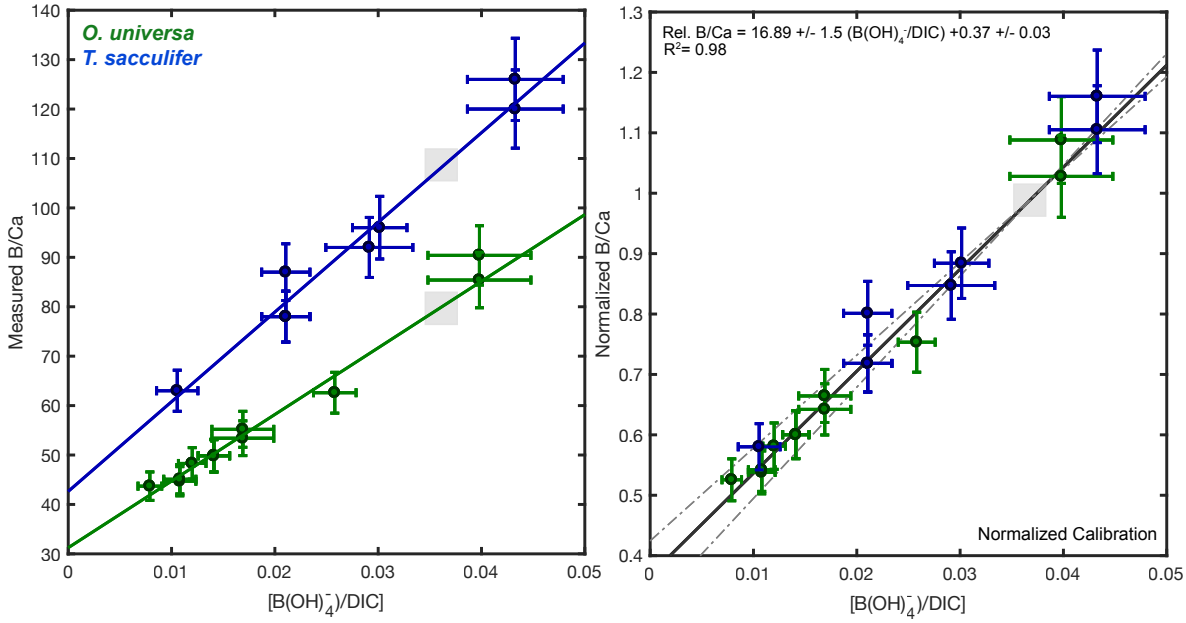

Figure S1. Normalized B/Ca calibrations for application to the PETM excursion. Raw B/Ca culture data of Haynes et al. (2017, 2019) from two modern species - *O. universa* and *T. sacculifer* - are shown in panel A. B/Ca data are then normalized to each species' B/Ca values at the calculated pre-PETM $[B(OH)_4^-/DIC]$ ratio of 0.037 (grey boxes, and panel B). In doing so, the calibration is scaled to assume a pre-PETM normalized B/Ca of 1 (grey box, panel B). The combined dual-species calibration with corresponding slope uncertainties is shown in panel B. Error bars reflect 2σ uncertainties on measured B/Ca and culture water $[B(OH)_4^-/DIC]$.

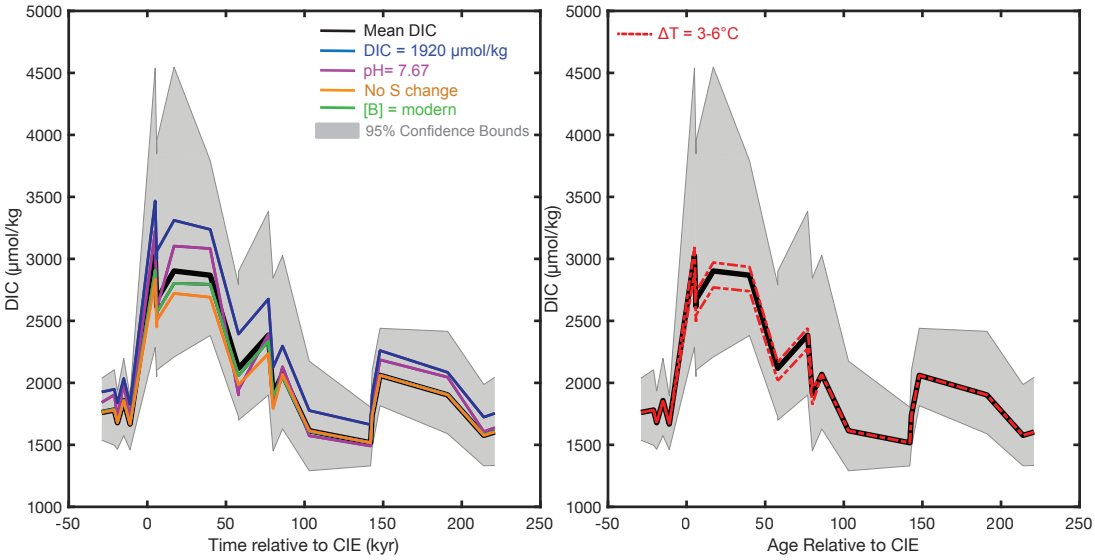

Figure S2. Effects of assumed input parameters (T, S, $[B]_T$, baseline pH and baseline DIC) on reconstructed DIC. In black, we show mean reconstructed DIC as in Fig. 1D. The colored lines reflect DIC scenarios that test the influence of the various input parameters for this calculation. The corresponding colors of individual sensitivity tests is as follows: blue, we assume a different starting DIC of 1920 µmol/kg, which is the value predicted by recent LOSCAR model runs (ref. 3); purple, we assume a lower background pH of 7.67 (ref. 3) rather than 7.8 (ref. 2); orange, we assume no change in S across the PETM; green, we assume a modern $[B]_T$ value (and thus slightly higher overall $[B(OH)_4^-]$ In the right-hand panel, we test the influence of assuming a temperature excursion of 3 or 6°C (ref. 1), compared to the 5°C excursion employed in our mean analysis (after ref. 12). In each of these cases, the assumed input parameter makes a small overall impact on reconstructed DIC. In the cases of starting pH and DIC, these alternate values predict increased DIC excursions.

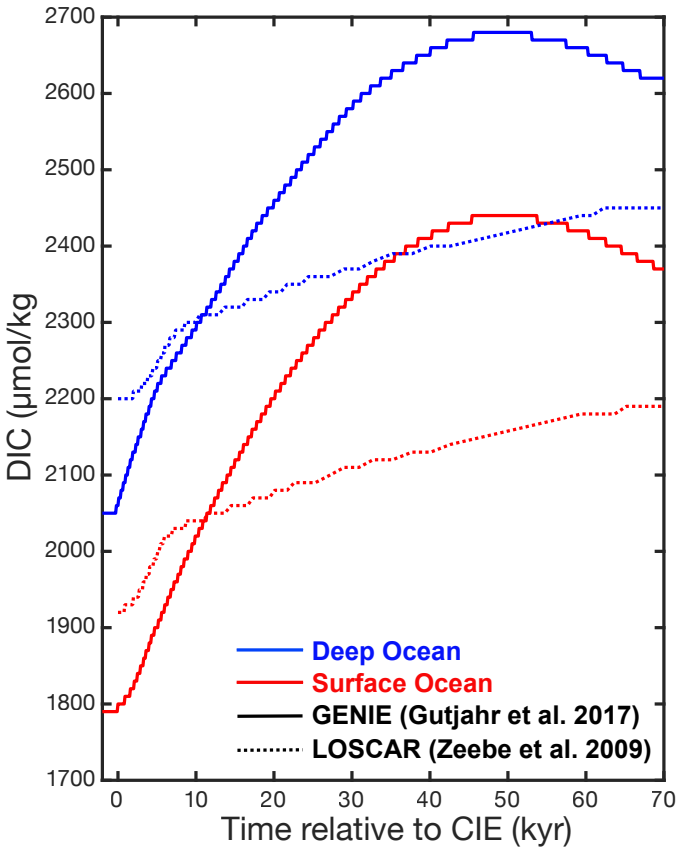

Figure S3. Earth System Model output of surface and deep-ocean DIC trajectories across the peak-PETM. Results from a cGENIE model run assuming a 10,000 PgC input are shown in solid lines (ref. 10), whereas results from a LOSCAR model run assuming a 3,300 PgC input are shown in stippled lines (ref. 20). In LOSCAR, the "surface" and "deep-ocean" output shown are from the model's shallow and deep Pacific boxes, respectively. In the case of the GENIE model output, we show the estimated global ocean surface and deep-ocean DIC response. While the definition of "surface" and "deep" ocean varies between the two models, we seek to show here that both models suggest similar timings of surface and deep-sea DIC increases from PETM carbon release simulations.

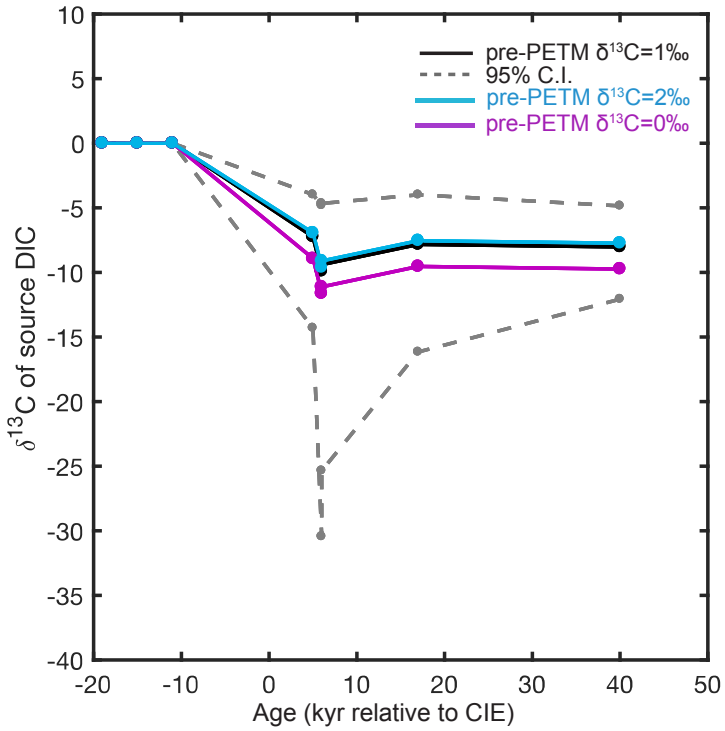

Figure S4. The influence of assumed pre-PETM $\delta^{13}C$ on reconstructed $\delta^{13}C_{source}$. Assuming a pre-PETM $\delta^{13}C$ of 2 or 0‰ (blue and purple lines, respectively) does not significantly change our conclusion that $\delta^{13}C_{source}$ likely included substantial contributions from volcanic carbon. 95% confidence intervals are derived from calculated $\delta^{13}C_{source}$ using lower and upper DIC bounds.

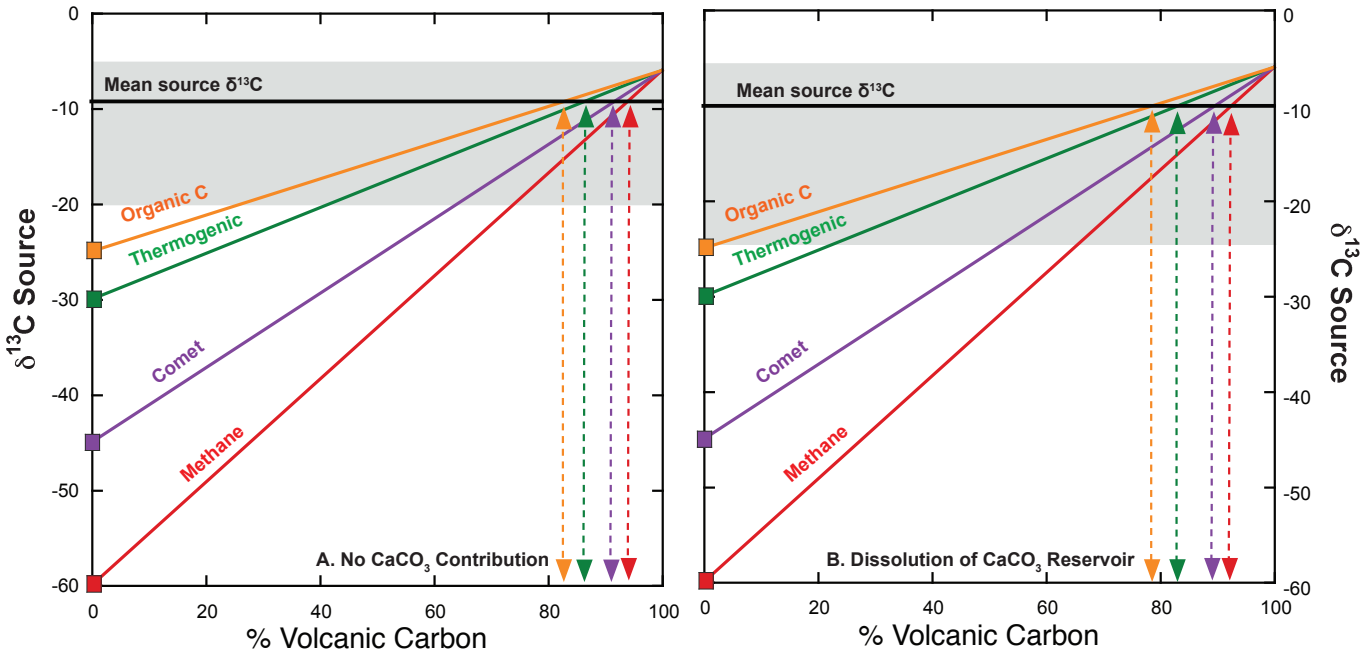

Figure S5. Mass contributions of volcanic carbon to PETM C release relative to possible secondary sources (methane, comet, thermogenic methane, and organic carbon). Mixing lines are shown as a function of the % volcanic carbon required to explain our mean reconstructed $\delta^{13}C_{source}$ (black line). Colored arrows correspond to the mean volcanic mass % contribution given the additional contribution of each secondary source (carbon derived from organic, thermogenic, comet, or methane sources). Volcanic carbon $\delta^{13}C$ is assumed at -6‰. In A, we show the possible volcanic mass contributions assuming that $\delta^{13}C_{source}$ is unaffected by $CaCO_3$ dissolution. In B, we show the maximum possible contribution of sedimentary $CaCO_3$ dissolution on $\delta^{13}C_{source}$ and the resultant mass contributions of volcanic C. Assuming the maximum contribution of dissolved $CaCO_3$ to $\delta^{13}C_{source}$ changes the mean possible volcanic contribution by a small amount (B). Our analysis implies that mean volcanic C contributions can account for 80-95% of the C added to the surface ocean at the PETM compared to the other sources.

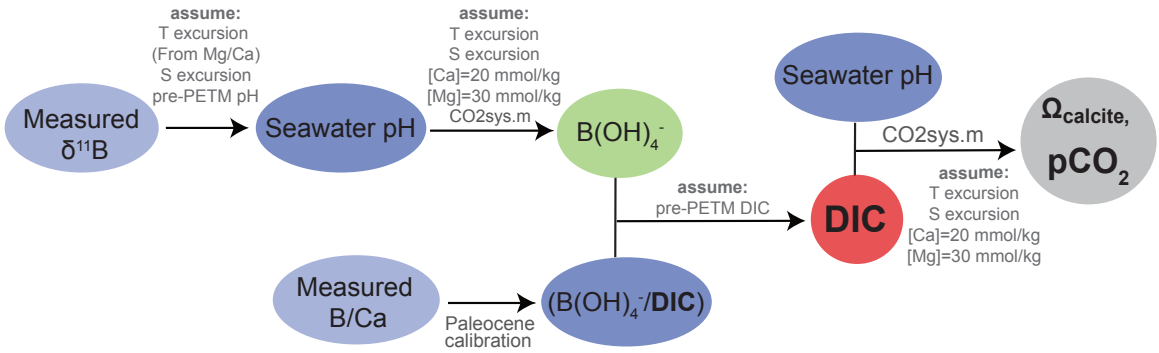

Figure S6. Calculation Schematic for determining DIC and full carbon system parameters. Adapted from Haynes et al. (2017). The assumptions utilized in each calculation step are included with each arrow.

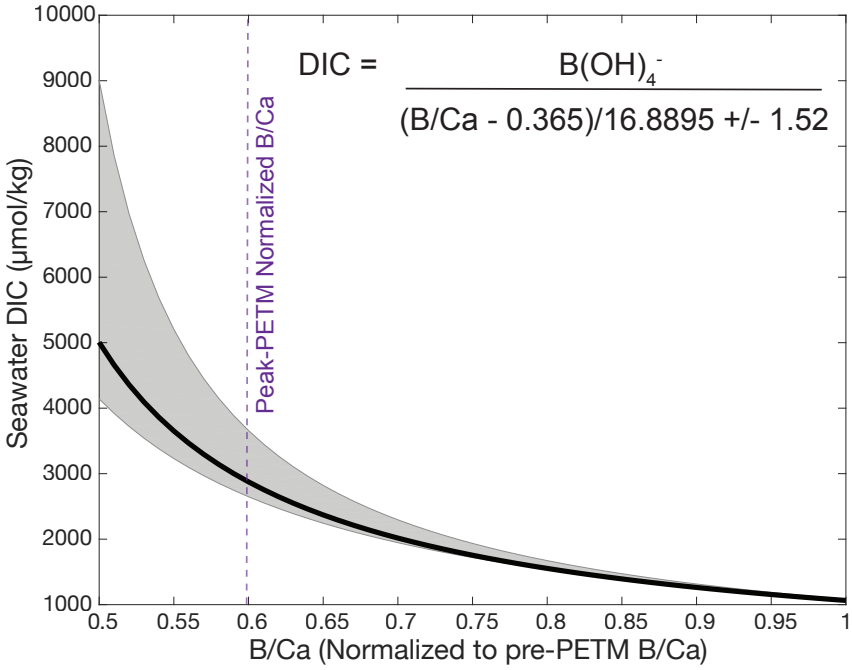

Figure S7. Demonstrated non-linearity of the DIC calibration at low normalized B/Ca (relative to pre-PETM B/Ca). When Monte Carlo simulation of errors reaches high DIC values, they are likely to be amplified by the reciprocal function (shaded 95% confidence region). In this illustrative case, we test the influence of slope uncertainty on reconstructed DIC and assume a constant $B(OH)_4^-$ of 40 µmol/kg.

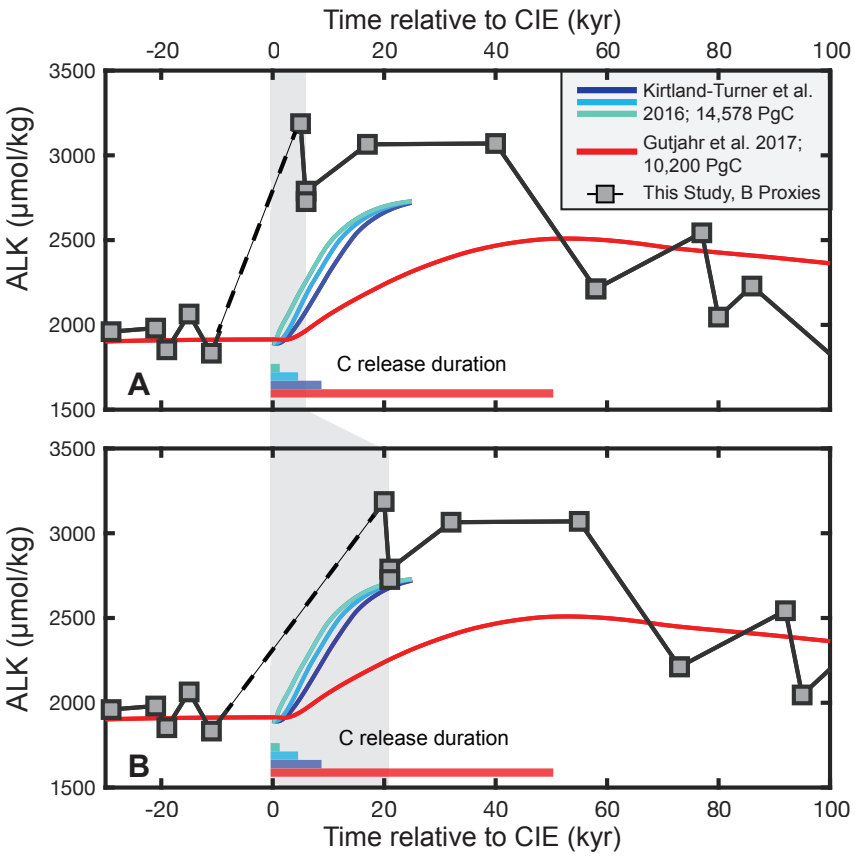

Figure S8. Modeled and reconstructed alkalinity change across the PETM. Symbol and line assignments are the same as those made in main text Fig. 4. Modeled alkalinity increases to a maximum at ~20-25 kyr post-CIE, regardless of C input duration time. Post-CIE B-proxy derived alkalinity is shifted by 15 kyr as in Fig. 4.

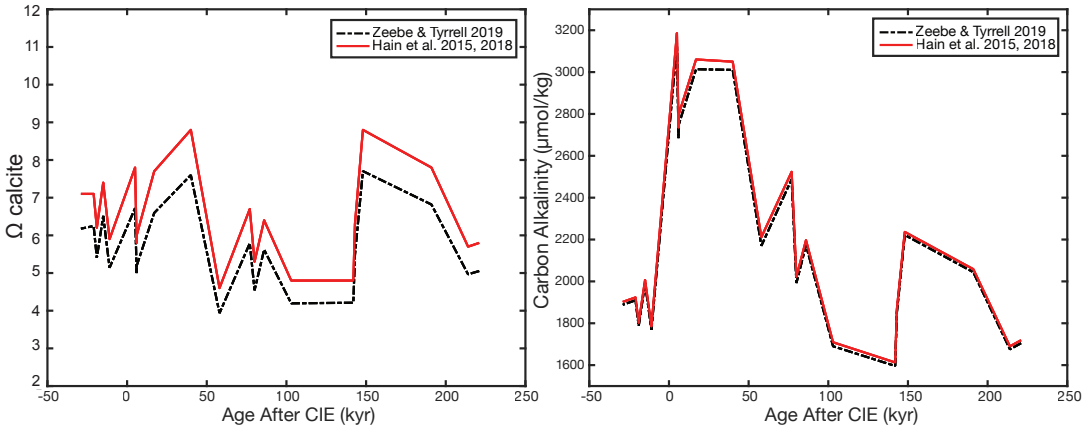

Figure S9. The influence of [Ca] and [Mg] on reconstructed carbon system parameters via the parameterization of carbon system dissociation constants. The black scenario shows the correction for K_1, K_2, and K_{sp} derived by Zeebe & Tyrrell (2019), while the red scenario reflects the Pitzer ion model formulation (PyMyAMI) of Hain et al. (2015, 2018).

SI References

1. Dunkley-Jones, T., Lunt, D. J., Schmidt, D. N., Ridgwell, A., Sluijs, A., Valdes, P. J., & Maslin, M. (2013). Earth-Science Reviews Climate model and proxy data constraints on ocean warming across the Paleocene – Eocene Thermal Maximum. *Earth Science Reviews*, *125*, 123–145. http://doi.org/10.1016/j.earscirev.2013.07.004

2. Panchuk, K., Ridgwell, A., & Kump, L. R. (2008). Sedimentary response to Paleocene-Eocene thermal maximum carbon release: A model-data comparison. *Geology*, *36*(4), 315–318. http://doi.org/10.1130/G24474A.1

3. Zeebe, R. E., Zachos, J. C., & Dickens, G. R. (2009). Carbon dioxide forcing alone insufficient to explain Palaeocene – Eocene Thermal Maximum warming. *Nature Geoscience*, *2*(8), 1–5. http://doi.org/10.1038/ngeo578

4. Lowenstein, T. K., Kendall, B., and Anbar, A.D. (2014). *Chapter 8 . 21 - The Geologic History of Seawater*. In *Treatise on Geochemistry 2nd edition.*

5. Lemarchand, D., Gaillardet, J., Lewin, E., & Allegre, C. J. (2000). The influence of rivers on marine boron isotopes and implications for reconstructing

past ocean pH. *Nature*, *408*(6815), 951–954. http://doi.org/Doi 10.1038/35050058

6. Evans, D., Sagoo, N., Renema, W., Cotton, L. J., Müller, W., & Todd, J. A. (2017). Eocene greenhouse climate revealed by coupled clumped isotope-Mg / Ca thermometry, *Proceedings of the National Academy of Sciences* 1–6. http://doi.org/10.1073/pnas.1714744115

7. Nunes, F. and Norris, R.D. (2006). Abrupt reversal in ocean overturning during the Palaeocene/Eocene warm period. *Nature* 439 (7072).

8. Kozdon, R., Kelly, D. C., and Valley, J.W. (2018). Diagenetic attenuation of carbon isotope excursion recorded by planktic foraminifers during the Paleocene-Eocene Thermal Maximum. Paleoceanography and Paleoclimatology 33(4).

9. McCarren, H.K., Thomas, E., Hasegawa, T., Röhl, U., and Zachos, J.C. (2008). Depth dependency of the Paleocene-Eocene carbon isotope excursion: Paired benthic and terrestrial biomarker records (Ocean drilling program Leg 208, Walvis Ridge). *Geochemistry, Geophysics, Geosystems* 9(10).

10. Elling, F., Gottschalk, J., Doeana, K., Kusch, S., Hurley, S.J., and Pearson, A. (2019). Archael lipid biomarker constraints on the Paleocene-Eocene carbon isotope excursion. *Nature Communications* 10:4519.

11. Gutjahr, M., Ridgwell, A., Sexton, P. F., Anagnostou, E., Pearson, P. N., Pälike, H., Norris, R.D., Thomas, E. and Foster, G. L. (2017). the Palaeocene – Eocene Thermal Maximum. *Nature* 548(7669), 573–577. http://doi.org/10.1038/nature23646

12. Ma, Z., Gray, E., Thomas, E., Murphy, B., Zachos, J., & Paytan, A. (2014). Carbon sequestration during the Palaeocene – Eocene Thermal Maximum by an e cient biological pump, *7*(May). http://doi.org/10.1038/NGEO2139

13. Penman, D., Hönisch, B. Zeebe, R., Thomas, E., and Zachos, J. (2014). Rapid and sustained surface ocean acidification during the Paleocene-Eocene Thermal Maximum. *Paleoceanography* 29, 1–13. http://doi.org/10.1002/2014PA002621.Received

Dataset S1 (separate file). Input parameters for PETM DIC calculation.

Dataset S2 (separate file). Reconstructed DIC from the B/Ca method.

Dataset S3 (separate file). Reconstructed carbon system parameters across the PETM record from boron isotope and B/Ca reconstructions.

Dataset S4 (separate file). Reconstructed $\delta^{13}C$-source values during the peak-PETM.

Dataset S5 (separate file). Reconstructed DIC using B/Ca excursions from other sediment core sites.